EOGE

EARTH OBSERVATION AND GEOMATICS ENGINEERING

website: https://eoge.ut.ac.ir

Preparation of flood susceptibility mapping using an ensemble of frequency ratio and adaptive neuro-fuzzy inference system models

S. Vahid Razavi-Termeh, Abolghasem Sadeghi-Niaraki *

Geoinformation Tech, Center of Excellence, Faculty of Geomatics, K.N. Toosi University of Technology, Tehran, Iran

ABSTRACT

Floods are among the most common natural disasters that impose severe financial and human losses every year. Therefore, it is necessary to prepare susceptibility and vulnerability maps for comprehensive flood management to reduce their destructive effects. This study is trying to provide a flood susceptibility mapping in Jahrom (Fars Province) using a combination of frequency ratio (FR) and adaptive neuro-fuzzy inference system (ANFIS) and compare their accuracy. Totally, 51 flood locations areas were identified, 35 locations of which were randomly selected to model flood susceptibility and the remaining 16 locations were used to validate the models. Nine flood conditioning factors namely: slope degree, plan curvature, altitude, topographic wetness index (TWI), stream power index (SPI), distance from river, land use/land cover, rainfall, and lithology were selected, and the corresponding maps were prepared using ArcGIS. After preparing the flood susceptibility maps using these methods, the relative operating characteristic (ROC) curve was used to evaluate the results. The area under the curve (AUC) obtained from the ROC curve indicated the accuracy of 89% and 91.2% for the ensembles of FR and ANFIS-FR models, respectively. These results can be useful for managers, researchers, and designers in managing flood vulnerable areas and reducing their damages.

1. Introduction

Natural disasters such as landslip, earthquakes, and floods annually cause a lot of financial and financial losses all over the world (Tierney et al., 2002). Floods are one of the natural disasters whose imposed damage is not countable (Du et al., 2013; Lyu et al., 2018). Floods cause severe damage to transportation, cultural heritage, environmental ecosystems, economy, and human life (Yu & Larsen, 2013). Although it is impossible to prevent the occurrence of floods, it is possible to predict these catastrophic events, and to some extent, control those using appropriate methods and analyses (Cloke & Pappenberger, 2009; Farina et al., 2018). Also, the necessary measures to prevent floods and mitigate its adverse effects seem inevitable (Alvarado-Aguilar et al., 2012; Dang et al., 2011; Huang et al., 2008), one of which is the development of flood susceptibility mapping (Bubeck et al., 2012). According to Norouzi & Taslimi (2012), in Iran,

floods and their imposing damage are increasing every year, insofar the last decade's damage has increased by 250 percent. Accordingly, the occurrence of flood-related disasters is expected to increase because of the lack of urbanization, increasing deforestation, and continuous rainfall due to climate change in susceptible areas. The adverse effects of floods necessities the identification of flood-prone areas (Tehrany et al., 2015). Creating a flood susceptibility map as an undeniable need is the first step in preventing and managing future floods (Wu et al., 2010; Saidi et al., 2019). Growing access to satellite data, remote sensing, and business intelligence has increased the use of geographic information system (GIS) to prepare flood susceptibility mapping. Artificial neural networks (ANN) (Kia et al., 2012), analytical hierarchy process (AHP) (Chen et al., 2011), frequency ratio (FR) (Lee et al., 2012), logistic regression (LR) (Pradhan, 2010), and fuzzy logic (Pierdicca

---

et al., 2010) can be mentioned as some of the methods used to generate GIS-based flood susceptibility maps. Today, powerful machine learning methods, such as adaptive neuro-fuzzy (Mukerji et al., 2009), genetic algorithm (Chau et al., 2005), decision tree (DT), and support vector machine (SVM) (Adeli & Hung, 1994) have replaced traditional methods. Many of these methods have been rarely used in flood modeling, while they are highly able to cope with other natural disasters such as landslides (Pradhan, 2013; Yilmaz, 2010; Tien Bui et al., 2019). The mentioned models, when applied alone, have weaknesses and limitations in modeling. For instance, ANFIS (or other similar data mining and machine learning methods) has to deal with inconsistent input values. It also should cope with input error values due to the type of inputs in which the weight of each class of criteria is estimated through this method. As the case study, the Jahrom town is suffering from extreme seasonal floods that have always damaged the city. The purpose of this study is to prepare a flood susceptibility map for the Jahrom town by an ensemble of frequency ratio and adaptive neuro-fuzzy inference system.

2. Study area

The Jahrom Basin, with an area of about 5,737 Km^2, is located in the Jahrom county in the Southern Fars Province. The region is situated within 28° 17' to 29° 8' N latitudes and 54° 4' to 52° 45' E longitudes (Figure 1), with maximum and minimum elevations of 766 m and 3,166 m respectively. The natural landscape of this area is highly mountainous. Approximately one-fifth of the county comprises open fields and the rest are highlands. The average elevation of the area is about 1,050 m, and the highest point corresponds to the Safidar summit located between Khafr and Simakan with an elevation of 3,170 m. The lowest point with a height of about 766 m is located in Simakan. January is the coldest month in the area with an average temperature of about 10 °C and July is the warmest month with an average temperature of about 33 °C.

3. Materials and methods

3.1. Flood inventory map

The primary sources of flooding in the study area are torrential rains, changes in land use, especially in farmlands, as well as the lack of necessary measures to prevent floods. The most devastating floods in the region in the last decade happened in 2010 and 2017. The information on these floods was obtained from the Jahrom Department of Natural Resources. The 2017 flood caused extensive financial losses and casualties due to prolonged and intense rainfalls that lasted seven days. Among these damaged, three people were dead, several bridges were destroyed, and a village thoroughly drowned underwater in the path of the flood.

Flood dispersion maps are considered as an effective factor in flood prediction. In the Jahrom town, a total of 51 flood occurrences were recorded by the Fars Regional Water Company from 2011 to 2017, 35 of which (70%) were randomly selected to prepare flood susceptibility maps and the remaining 16 locations (30%) were used for model validation (Pourtaghi et al., 2014). The annual frequency of floods is shown in Figure 2, with the highest occurrence in 2017 with 12 occurrences.

3.2 Flood conditioning factor

One of the essential elements in the preparation of a flood susceptibility map is determining the factors influencing the flood (Kia et al., 2012). In this research, nine factors including slope degree, altitude, plan curvature, rainfall, distance from river, land use/land cover, lithology, SPI, and TWI were used (Tehrany et al., 2015; Tien Bui et al., 2019). ArcGIS 10 and QGIS 2.16.1 packages were used to provide information layers. First, a digital elevation model (DEM) with a resolution of 30*30 m was prepared from ASTER images, and accordingly, three factors including slope degree, altitude, and plan curvature were directly extracted from the DEM using ArcGIS. The topographic elevation is an effective factor in flood studies. It is almost impossible to face flooding in high elevated regions. Low-lying areas have high potential for flood occurrence. Water flows from hillsides of the mountains and joins in lower terrains in the rivers that will eventually cause flooding (Tehrany et al., 2015). Water-related factors such as SPI and TWI were also calculated from the DEM in QGIS following Eqs. (1) and (2) (Moore et al., 1991; Jaafari et al., 2014; Nampak et al., 2014).

$$TWI = \ln(\frac{A_s}{\beta}) \tag{1}$$

$$SPI = A_s \tan \beta \tag{2}$$

where, As and β denote the area of a specific basin (m²/m) and the slope degree, respectively. The TWI factor shows the cumulative flow of a specific watershed in response to the pull of gravity which tends to lead the water to areas with lower slope angles (Moore et al., 1991). The distance from the river is another major factor that has a significant impact on the dimension and extent of the flood (Rahmati et al., 2016). Land use plays an essential role in the flooding process that directly or indirectly affects other hydrological processes such as permeability, evapotranspiration, and runoff production (Pourghasemi et al., 2012). The land use map of the area was provided by the Natural Resources Department of Fars Province at a scale of 1:100,000. In general, rangeland, farmlands, and low-density forests are the dominant land covers in the study area. Residential areas, which are built mainly by impermeable surfaces, have increased runoffs and river flooding (Rahmati et al., 2016).
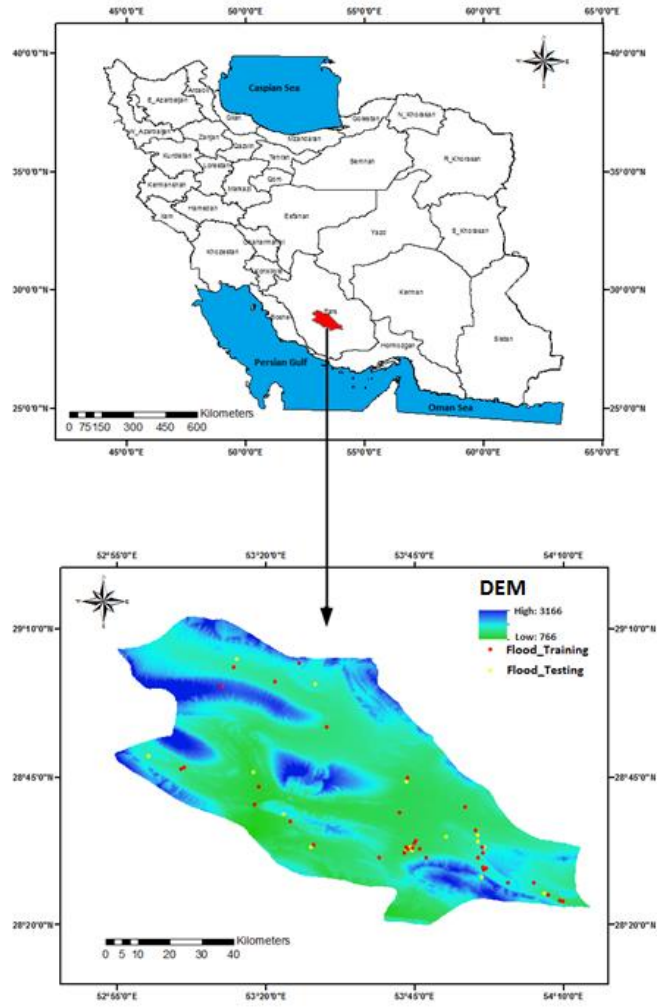
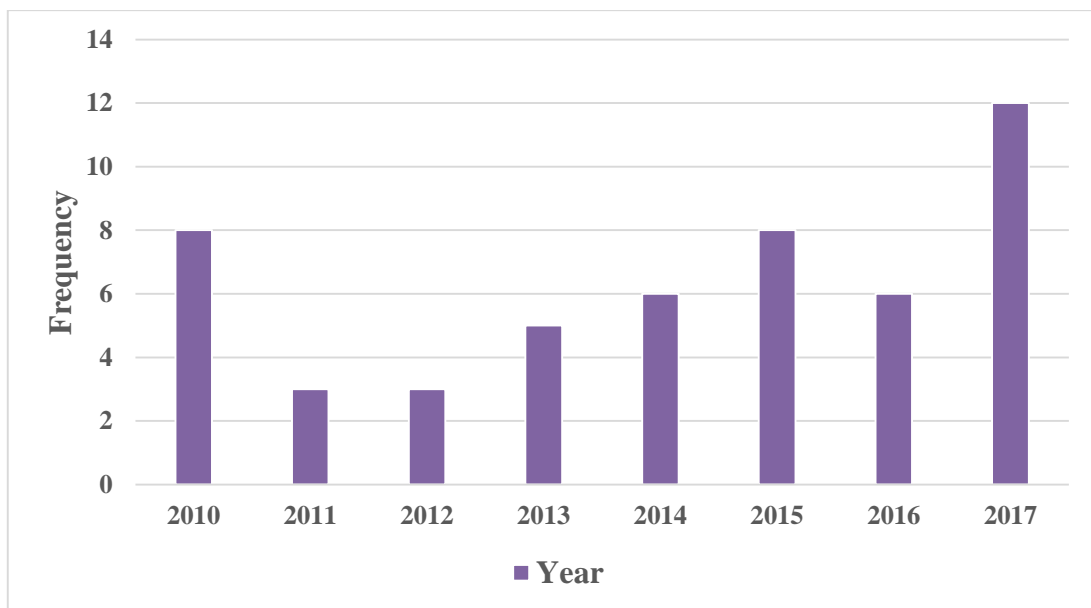Figure 1. Floods distribution map of the study area

Figure 2. Annual frequency of floods

Also, the areas with low-density vegetation cover are prone to flooding due to the positive relationship between the permeability and the cover density. In general, lithological features of the region plays a significant role in the preparation of a flood susceptibility map because many of lithological units are active in hydrological processes (Miller, 1990). The region with resistant rocks or semi-permeable units has a less developed drainage system, thus lower ability of flood absorption (Srivastava et al., 2014). The lithology layer was prepared from the 1:100000 geological map of the area. Alluvial units (Qft2) form the dominant lithological units in the study area. The information layers of flood conditioning factors are shown in Figure 3. Table 1 presents the characteristics of the lithology layer.

Table 1. The description of lithological formations in the study area

Code	Lithology	Geological age
Qft2	Low-level piedmont fan, valley terrace deposit	Cenozoic
EOas-ja	Undivided Asmari and Jahrom Formation	Cenozoic
Kgu	Bluish grey marl and shale with subordinate thin-bedded argillaceous -limestone	Mesozoic
PeEsa	Pale red marl, marlstone, limestone, gypsum and dolomite	Cenozoic
Kepd-gu	Massive fossiliferous limestone	Cenozoic
Plbk	Conglomerate locally with sandstone	Cenozoic
MuPlaj	Sandstone (brown to gray), red marl, siltstone	Cenozoic
Kbgp	Bangestan Group: mainly limestone and shale	Mesozoic
OMr	Red, grey, and green silty marls interbedded with subordinate silty limestone and minor sandstone ribs	Cenozoic
pC-Ch	Rock salt, gypsum & blocks of contorted masses of sedimentary material such as black laminated fetid limestone, brown cherty dolomite, red sandstone & variegated shale in association with igneous rocks such as diabase, basalt, rhyolite, and trachyte	Paleozoic
Ktb	Massive, shelly, cliff-forming partly anhydrite-bearing limestone	Mesozoic
OMas	Jointed limestone with intercalation of shale	Cenozoic
Mmn	Low weathering gray marls alternating with bands of more resistant shelly limestone	Cenozoic
JKkgp	Undivided Khami Group, consist of massive thin-bedded limestone comprising the following formations: Surmeh, Hith Anhydrite, Fahlian, Gadvan, and Dariyan	Mesozoic

Figure 3. Effective measures on floods in the study area: (a) curvature, (b) lithology, (c) altitude, (d) land use, (e) rainfall, (f) distance from river, (g) slope degree, (h) SPI, (i) TWI
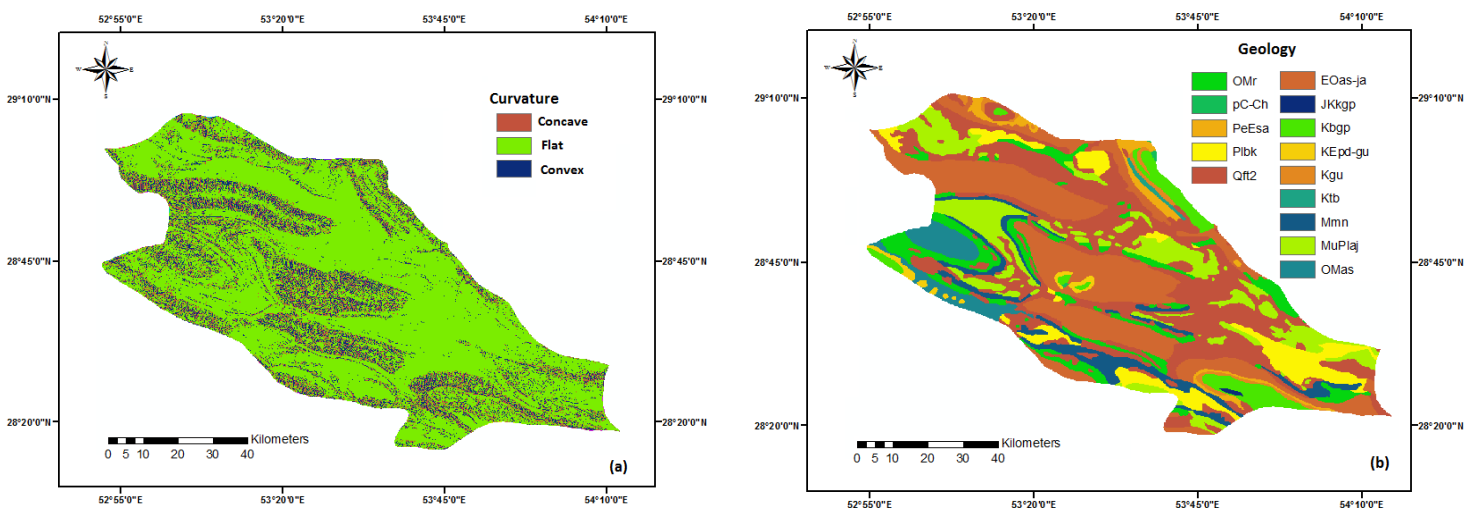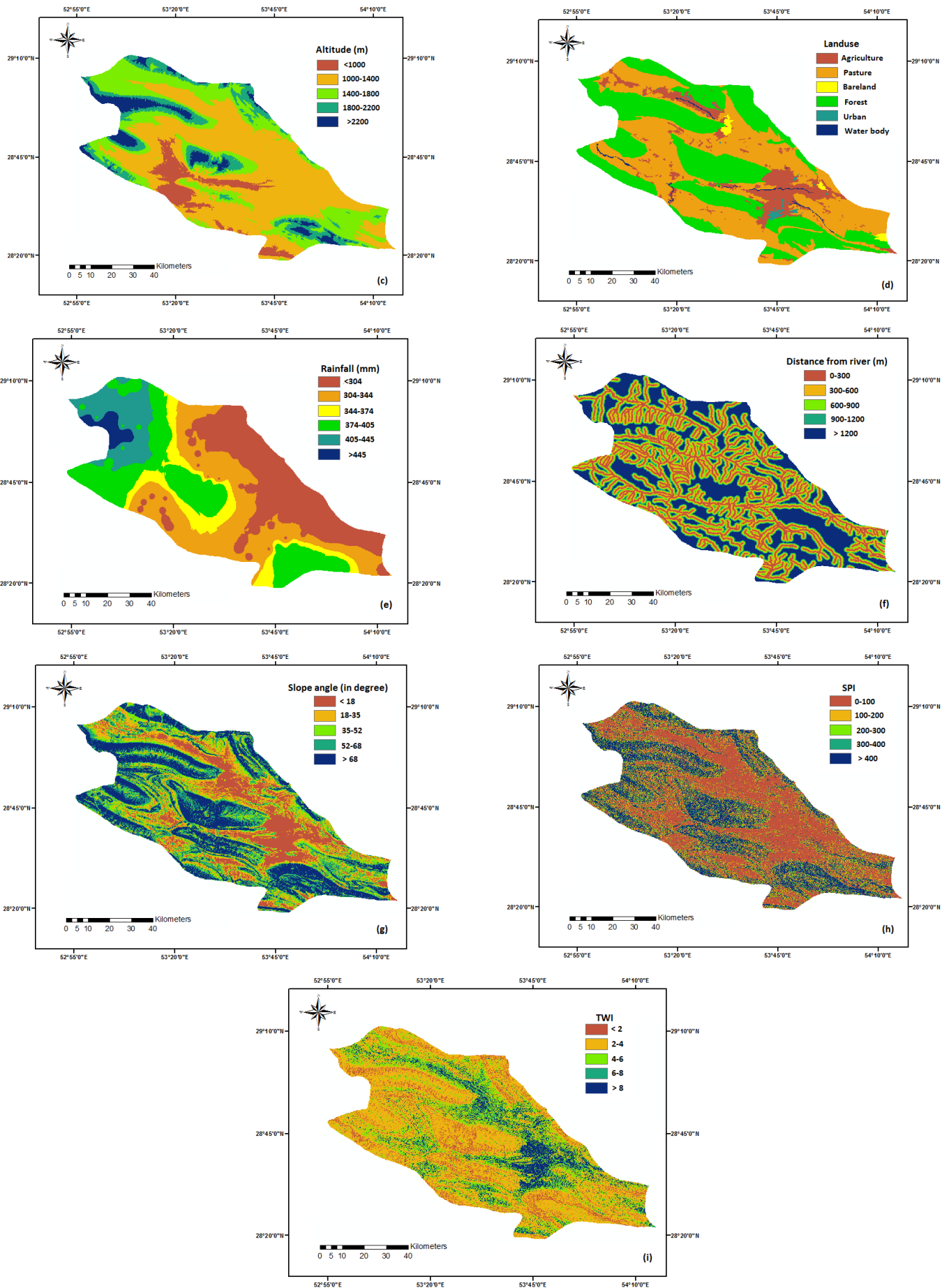
Figure 3. Effective measures on floods in the study area: (a) curvature, (b) lithology, (c) altitude, (d) land use, (e) rainfall, (f) distance from river, (g) slope degree, (h) SPI, (i) TWI (Continued)

3.3. Models

3.3.1. Frequency ratio (FR) model

The FR model, as a bivariate statistical model, can be used as a simple spatial tool to calculate the probabilistic relationship between independent and dependent variables, which includes several categorized maps (Oh et al., 2011). This method was used to prepare a groundwater potential mapping map by Ozdemir (2011). The FR value of occurrence probability for a phenomenon is in the presence of a specific property. The FR approach is based on the observed relationship between the distribution of flood and flood conditioning factors. The FR of each layer is calculated from each criterion according to Eq. (3).

$$FR = \frac{A/B}{C/D} \qquad (3)$$

In this equation, A is the number of pixels with floods for each factor, B is the total number of floods in the study area, C is the number of pixels per layer of each factor, and D is the total number of pixels in the study area, FR is the frequency ratio from the layer for each factor.

3.3.2 Adaptive Neuro-Fuzzy Inference System (ANFIS)

Although fuzzy models cannot be trained, they have the knowledge and ability to display complex processes by applying the IF-THEN concepts and rules. Besides, if the number of input variables in the description of a problem is high, choosing the membership functions and IF-THEN rules fit in the fuzzy model is very difficult, and the phase-setting phase of the fuzzy model will be endless (Bui et al., 2012). In this method, the learning algorithm automatically selects the appropriate parameters for membership functions in the fuzzy model. Although neural networks are capable of learning, they are not able to describe the systems; therefore, an adaptive neuro-fuzzy inference system is used (Polat & Gunes, 2006). Among other abilities of the model, which will broadly outperform the fuzzy model, it is also self-contained. In general, ANFIS uses a hybrid learning principle that combines the gradient and the least-squares method to determine the parameters (Wang & Elhang, 2008). The ANFIS structure presented in this study is shown in Figure 4 (Bui et al., 2012).

According to Figure 4, the layers in an ANFIS model are defined as follows. For layer 1, each node contains adaptive variable nodes [Eqs. (4) and (5)]:

$$O_{1,i} = \mu A_i (x) \qquad (4)$$

$$O_{1,i} = \mu B_i (y) \qquad (5)$$

where, x and y are the input nodes, A and B are the linguistic variables, and $\mu A_i(x)$ and $\mu B_i(y)$ are membership functions for that node.

Layer 2 contains fixed nodes denoted as л in Figure 4. Every node has the role as a "fuzzy AND' operation, that used for firing strength calculation of the rules as the output layer. The output of each node is the product of all input signals to that node [Eq. (6)]:

$$O_{2,i} = W_i = \mu A_i(x)\mu B_i(y), i = 1,2 \qquad (6)$$

where, W_i is the output for each node.

The third layer encompasses a set of fixed nodes showed as an N symbol in Figure 4. The nodes in this layer are in fact, the normalized outputs of layer 2 referred to as the normal firepower [Eq. (7)]:

$$O_{3,i} = \bar{w}_l = \frac{w_i}{w_1 + w_2}, i = 1,2 \qquad (7)$$

Each node in layer 4 is associated with a node function [Eq. (8)]:

$$O_{4,i} = \bar{w}_l f_i = \bar{w}_l (p_i x + q_i y + r_i) \qquad (8)$$

where, $\overline{w_l}$ is the normalized firepower of layer 3 and p_i, q_i, and r_i are node parameters. The parameters of this layer can be interpreted as the result parameters.

The fifth layer contains a single node denoted as ∑ which is the sum of the fourth layer output values and shows the final result of the ANFIS model, which is shown as follows: [Eq. (9)]:

$$O_{5,i} = \sum \bar{w}_l f_i = \sum w_i f_i / \sum w_i, i = 1,2 \qquad (9)$$

4. Results and discussion

The results of the spatial interaction between flood occurrence and related conditioning factors using the FR model is summarized in Table 2. The percentage of each class is obtained by dividing the number of pixels in each class by the total number of pixels of that factor. An analysis of the frequency ratio between flood and plan curvature showed that the flat class has the highest frequency ratio (1.10) and then the concave class has a value of 1.03. The results regarding the altitude factor showed that the highest frequency ratio belonged to 1,000 1,400 m class (1.48), followed by 0 1,000 m class (1.21). The first 300 meters from the rivers had the highest frequency ratio (2.30). The results regarding slope degree showed that more than 50% of flood events occurred within the range 0-18 degrees with a frequency ratio of 3.06. As for the rainfall factor, the range 304 344 mm had the highest frequency ratio (2.03), followed by the range 344-374 mm (1.42). Regarding the results of land use/land cover factor, residential areas and water bodies had the highest frequency ratio with respective values of 29.15 and 20.82. The highest frequency ratio for lithological formations related to Qft2 (1.78), followed by Mmn (1.43) and OMr (1.03) formations, respectively. As for SPI factor, the highest frequency ratio related to the range of 300-400

(1.45), followed by the range of 0-100 (1.31). TWI results showed that the highest frequency ratio belonged to the values ≥8 (3.7), where about 45% of flood events occurred in this category. After assigning weights to the factor classes, the flood susceptibility map was prepared using ArcGIS. The resulted map was classified into five susceptibility categories namely very low, low, medium, high, and very high susceptibility (Figure 5).
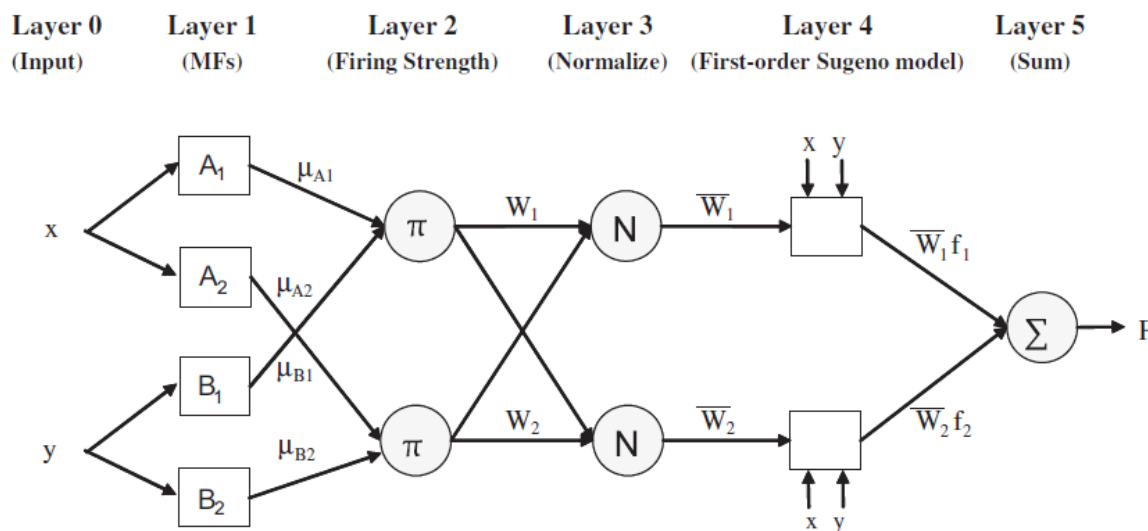

Figure 4. The structure of ANFIS model

Table 2. The spatial relationship between flood conditioning factors and flood locations using the FR method

Class	No. of pixels in domain	Percentage of domain	No. of floods	Percentage of floods	FR
Plan curvature					
Concave	32431	11.05	4	11.42	1.03
Flat	220921	75.27	29	82.86	1.10
Convex	40119	13.68	2	5.72	0.42
Altitude (m)					
0-1000	20699	7.04	3	8.58	1.22
1000-1400	141216	48.07	25	71.42	1.49
1400-1800	78627	26.8	6	17.14	0.64
1800-2200	35008	11.91	0	0	0.00
> 2200	18158	6.18	1	2.86	0.46
Distance from river (m)					
0-300	69266	23.58	19	54.29	2.30
300-600	59982	20.42	5	14.28	0.70
600-900	47281	16.1	3	8.58	0.53
900-1200	34629	11.8	4	11.42	0.97
>1200	82550	28.1	4	11.43	0.41
Slope angle					
0-18	52055	17.74	19	54.28	3.06
18-35	51030	17.38	5	14.29	0.82
35-52	49192	16.77	2	5.71	0.34
52-68	57751	19.68	6	17.14	0.87
>68	83443	28.43	3	8.58	0.30
Rainfall (mm)					
0-304	81339	27.71	6	17.14	0.62
304-344	78364	26.7	19	54.28	2.03
344-374	29379	10.02	5	14.29	1.43
374-405	67643	23.05	3	8.57	0.37
405-445	29824	10.16	2	5.72	0.56
>445	6911	2.36	0	0	0.00
Land use/land cover					
Agriculture	32513	11.07	4	11.43	1.03
Pasture	133759	45.54	15	42.85	0.94
Bare land	2253	0.77	0	0	0.00
Forest	121441	41.34	5	14.29	0.35
Urban	1727	0.59	6	17.14	29.15
Water body	2015	0.69	5	14.29	20.82

Table 2. The spatial relationship between flood conditioning factors and flood locations using the FR method (Continued)

Class	No. of pixels in domain	Percentage of domain	No. of floods	Percentage of floods	FR
Lithology					
Qft2	84940	28.9	18	51.42	1.78
EOas-ja	71756	24.43	7	20.02	0.82
Kgu	3419	1.286	0	0	0.00
PeEsa	6445	2.2	0	0	0.00
Kepd-gu	2493	0.85	0	0	0.00
Plbk	21492	7.3	2	5.71	0.78
MuPlaj	37827	12.8	2	5.71	0.44
Kbgp	11186	3.8	0	0	0.00
OMr	24365	8.3	3	8.57	1.03
pC-Ch	238	0.08	0	0	0.00
Ktb	968	0.33	0	0	0.00
OMas	10735	3.65	0	0	0.00
Mmn	17567	5.98	3	8.57	1.43
JKkgp	277	0.094	0	0	0.00
SPI	134167	45.68	21	60	1.31
0-100	40692	13.85	5	14.28	1.03
100-200	26518	9.02	1	2.85	0.32
200-300	17255	5.89	3	8.58	1.46
300-400	75076	25.56	5	14.29	0.56
>400					
TWI					
0-2	27913	9.5	1	2.85	0.30
2-4	157391	53.58	11	31.45	0.57
4-6	62694	21.34	6	17.14	0.80
6-8	9468	3.24	1	2.85	0.89
>8	36242	12.34	16	45.71	3.70

After normalizing the FR values (Table 2), these weights were introduced into the MATLAB application for the implementation of the adaptive fuzzy inference system. In this step, a c-mean clustering fuzzy inference system with a Gaussian function, genfis2, and a hybrid back-propagation algorithm was used to optimize and train the model. The results of training and test data related to the ANFIS model are shown in Figure 6. The RMSE value for ANFIS-FR model is 0.32. After the model was trained and finalized, the generalized region was extended over the entire area, and the final file was transmitted to MATLAB's text format into ArcGIS to provide the flood susceptibility map. Finally, the flood susceptibility map was prepared in the GIS environment and was divided into five very low to very high levels. Flood susceptibility map using this method is shown in Figure 7. An example of the training dataset is presented in Table 3.

Table 3. An example of the training dataset

| TWI	SPI	Slope	Distance to river	Rainfall	Land use	Altitude	Lithology	Plan curvature
3.70	1.31	3.06	2.32	0.562	1.03	1.4858	1.77	1.10
0.58	1.31	0.8715	0.69946	0.562	0.34	0.462	0.817	1.03
0.30	0.55	0.301	2.30	0	0.34	0.4621	0.818	1.100
0.58	0.55	0.3013	0.40	0	0.34	0.462	0.81	1.1
0.58	1.31	0.821	2.30	0.37	20.82	1.48	1.43	1.1
3.70	1.31	3.06	2.301	2.03	20.82	1.485	1.77	1.105
0.58	1.313	0.301	0.532	0	0.345	0	0.81	1.1
0.80	0.5581	0.301	0.699	0.37	0.3455	0	0.81	1.034
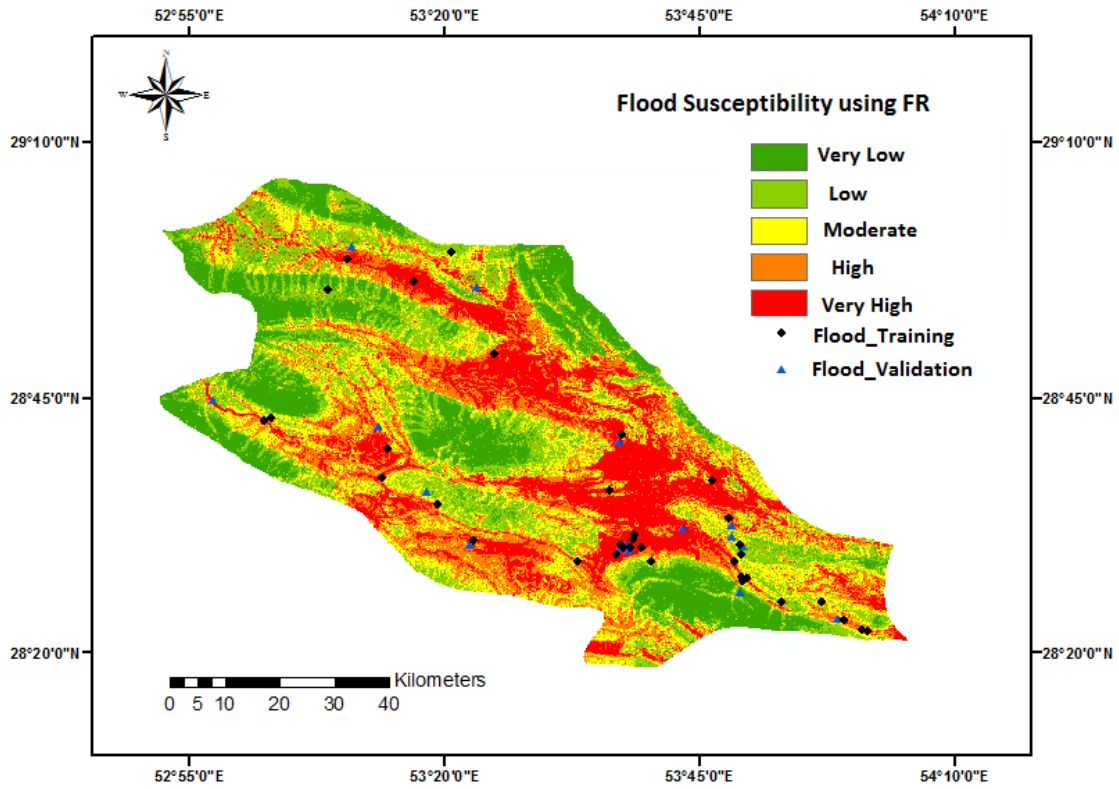
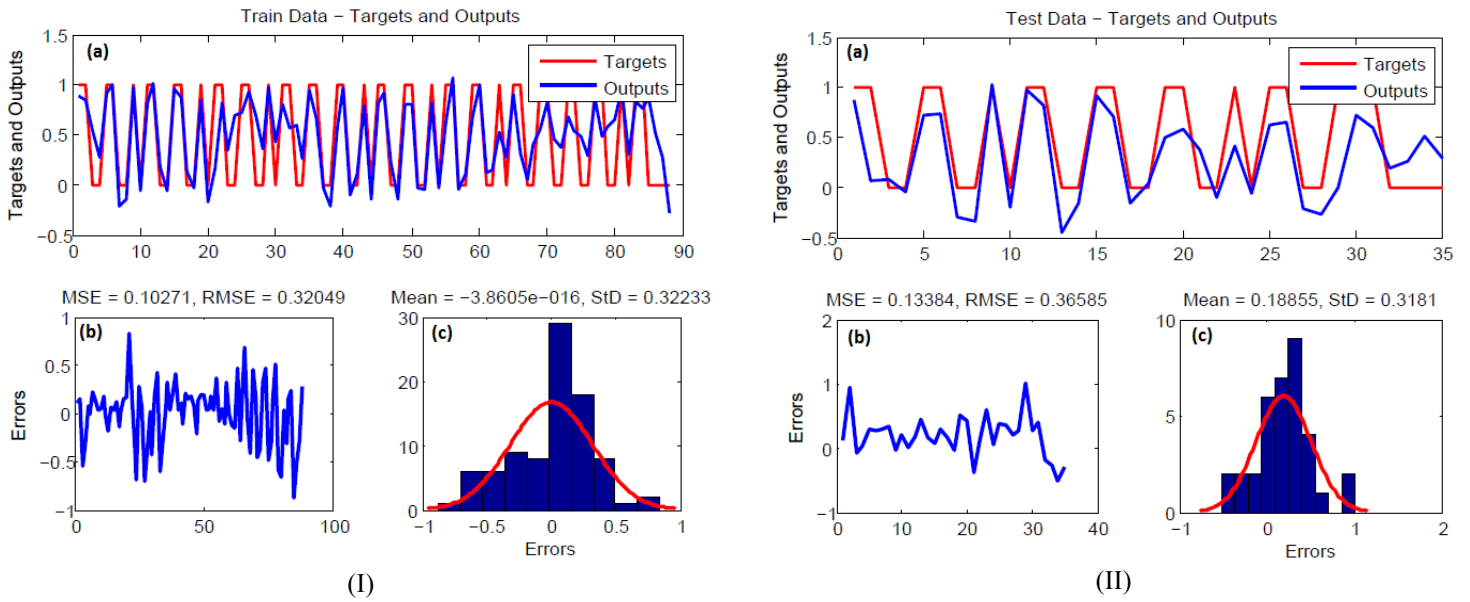Figure 5. Flood susceptibility map of the study area using the FR model

Figure 6. ANFIS-FR models I) Train data II) Test data: (a) target and output values, (b) MSE and RMSE values, and (c) Frequency errors
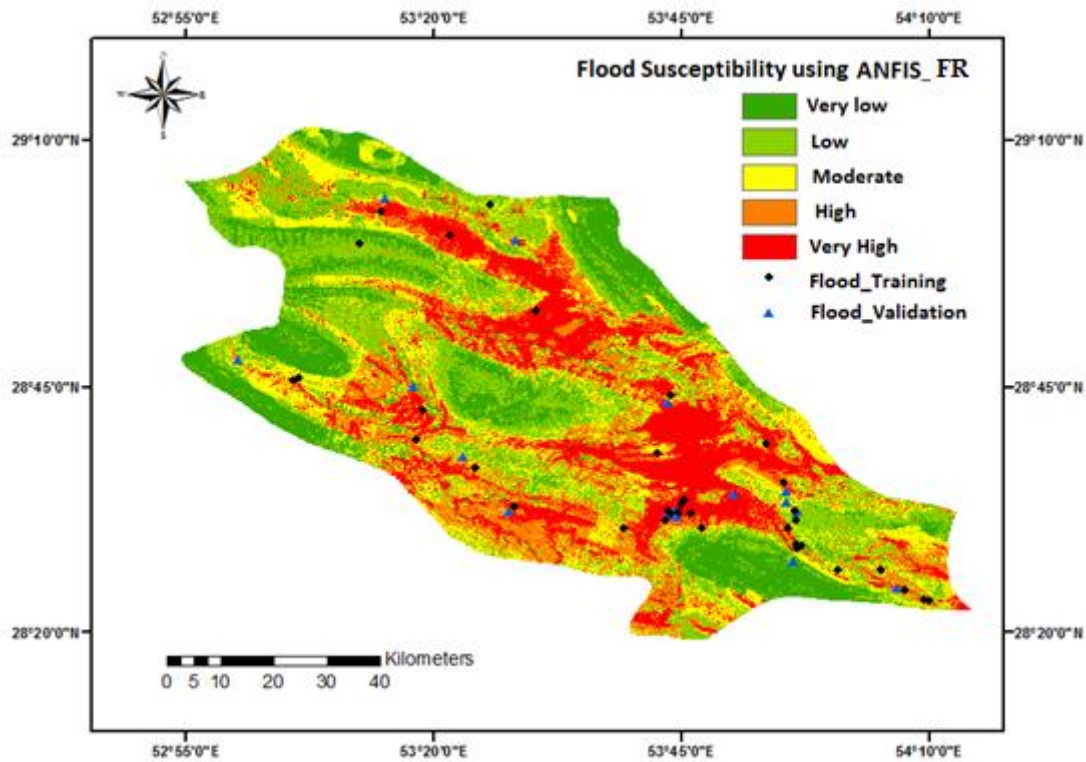
Figure 7. Flood susceptibility map of the study area using ANFIS-FR model

5. Validation

After preparing the final map of the two methods, the final map is divided into five very low to very high classes. In order to evaluate the prepared maps and their accuracy, it is not possible to use floods used in modeling because the use of these floods in the evaluation process does not accurately reflect the accuracy of the model. Also, the performance of the model should be assessed with the datasets that are not used for modeling (Komac, 2006). In order to solve this problem, several flood locations in the study area were used for modeling, and some of them were used to evaluate the model (70% and 30%, respectively) (Constantin et al., 2011). Then, the accuracy of the maps was confirmed using the ROC curve. The ROC curve is a graphical representation of the equilibrium between the negative and positive error rates for any potential value of the cutoff errors. The relative operating index is a curve who's vertical and horizontal components are calculated from Eqs. 10 and 11, respectively, derived from the confusion matrix with the definition of the threshold between zero and one. The values of the true positive percentage and the false positive percentage of the graph are calculated according to the following Equations (Komac, 2006):

$$X = 1 - \left[\frac{TN}{TN + FP} \right] \qquad (10)$$

$$Y = \left[\frac{TP}{TP + FN} \right] \qquad (11)$$

The area under the ROC curve, called AUC, represents the system's predictive value by describing its ability to correctly estimate the occurrence of an event (flood) and non occurrence (flood non occurrence). The ideal model is the highest area under the curve, whose AUC values vary from 0.5-1. If a model cannot estimate the flood event better than the probability (random), then its AUC is 0.5. When the area under the ROC curve is 1, it represents the best precision of the susceptibility map provided. Qualitative quantitative correlation below the curve and estimation assessment is as follows (0.9-1 excellent, 0.8-0.9, very good, 0.7-0.8 good, 0.6-0.7 moderate, 0.5-0.6 poor) (Zhu & Wang, 2009). The results of the evaluation indicate an accuracy of 89% for the FR model and an accuracy of 91.2% for the ensemble of ANFIS-FR model. The ROC diagram of the FR and ANFIS-FR models is shown in Figure 8. The results show good accuracy of ensemble ANFIS-FR compared to the FR model.
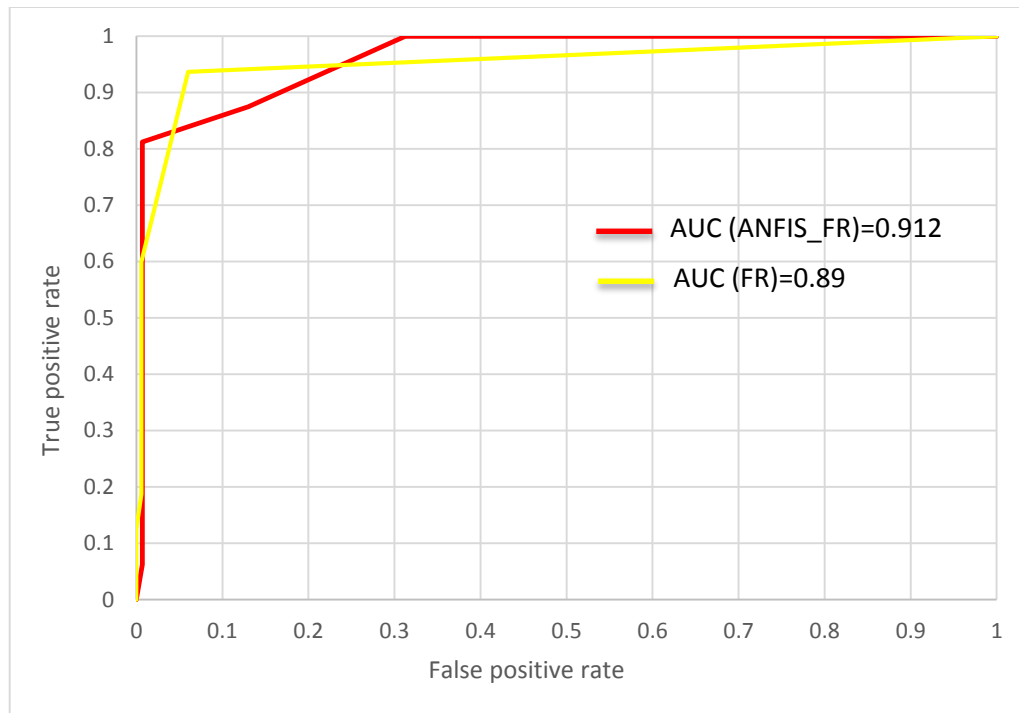
Figure 8. ROC curve related to FR and ANFIS-FR models

6. Conclusion

Floods are one of the most devastating natural disasters all over the world. Therefore, it is essential to prepare flood susceptibility maps for integrated management of watersheds in sustainable development. The need for a precise method to identify areas susceptible to flooding has led to the use of two models in this research to select the best regional model. In this research, flood susceptibility mapping was performed using the FR and ANFIS FR models. Initially, a flood inventory map containing 51 flood occurrence locations was prepared for the Jahrom town. Then, nine factors influencing the floods including slope degree, altitude, plan curvature, rainfall, distance from river, land use/land cover, lithology, SPI, and TWI were used. Afterward, using the flood location and the factors affecting the flooding process, the final weights of the model were obtained, and a map was prepared using ArcGIS. Then, in order to implement the ANFIS method, normalized data of the FR model was used, and the model was implemented using MATLAB 2017b. In order to provide a flood susceptibility map, the outputs of this method were transmitted to ArcGIS to prepare the final map. The ROC curve and the AUC value were used to validate the models. For this purpose, out of 51 flood locations, 35 locations (70%) were used as the training data and 16 locations (30%) were used for the validation. The results obtained from the FR and ANFIS-FR models indicate an accuracy of 89% and 91.2% respectively for these two models. The results of these two methods for preparing a flood susceptibility map demonstrate the high accuracy of combined methods compared to the FR model. The results of the present research can be of great help to the government, planners, and engineers in preventing and reducing the occurrence of flood.

References

Adeli, H., & Hung, S.-L. (1994). Machine learning: neural networks, genetic algorithms, and fuzzy systems: John Wiley & Sons, Inc.

Alvarado Aguilar, D., Jiménez, J. A., & Nicholls, R. J. (2012). Flood hazard and damage assessment in the Ebro Delta (NW Mediterranean) to relative sea level rise. Natural Hazards, 62(3), 1301-1321.

Bubeck, P., Botzen, W. J., & Aerts, J. C. (2012). A review of risk perceptions and other factors that influence flood mitigation behavior. Risk Analysis: An International Journal, 32(9), 1481-1495.

Bui, D. T., Pradhan, B., Lofman, O., Revhaug, I., & Dick, O. B. (2012). Landslide susceptibility mapping at Hoa Binh province (Vietnam) using an adaptive neuro-fuzzy inference system and GIS. Computers & Geosciences, 45, 199-211.

Chau, K., Wu, C., & Li, Y. (2005). Comparison of several flood forecasting models in Yangtze River. Journal of

Hydrologic Engineering, 10(6), 485-491.

Chen, Y.-R., Yeh, C.-H., & Yu, B. (2011). Integrated application of the analytic hierarchy process and the geographic information system for flood risk assessment and flood plain management in Taiwan. Natural Hazards, 59(3), 1261-1276.

Cloke, H., & Pappenberger, F. (2009). Ensemble flood forecasting: A review. Journal of Hydrology, 375(3-4), 613-626.

Constantin, M., Bednarik, M., Jurchescu, M. C., & Vlaicu, M. (2011). Landslide susceptibility assessment using the bivariate statistical analysis and the index of entropy in the Sibiciu Basin (Romania). Environmental earth sciences, 63(2), 397-406.

Dang, N. M., Babel, M. S., & Luong, H. T. (2011). Evaluation of food risk parameters in the day river flood diversion area, Red River delta, Vietnam. Natural Hazards, 56(1), 169-194.

Du, J., Fang, J., Xu, W., & Shi, P. (2013). Analysis of dry/wet conditions using the standardized precipitation index and its potential usefulness for drought/flood monitoring in Hunan Province, China. Stochastic Environmental Research and Risk Assessment, 27(2), 377-387.

Farina, G., Bernini, A., Alvisi, S., & Franchini, M. (2018). Preliminary GIS elaborations to apply rapid flood spreading models. EPiC Series in Engineering, 3, 684-691.

Huang, X., Tan, H., Zhou, J., Yang, T., Benjamin, A., Wen, S. W., . . . Fen, S. (2008). Flood hazard in Hunan province of China: an economic loss analysis. Natural Hazards, 47(1), 65-73.

Jaafari, A., Najafi, A., Pourghasemi, H., Rezaeian, J., & Sattarian, A. (2014). GIS-based frequency ratio and index of entropy models for landslide susceptibility assessment in the Caspian forest, northern Iran. International Journal of Environmental Science and Technology, 11(4), 909-926.

Kia, M. B., Pirasteh, S., Pradhan, B., Mahmud, A. R., Sulaiman, W. N. A., & Moradi, A. (2012). An artificial neural network model for flood simulation using GIS: Johor River Basin, Malaysia. Environmental earth sciences, 67(1), 251-264.

Komac, M. (2006). A landslide susceptibility model using the analytical hierarchy process method and multivariate statistics in perialpine Slovenia. Geomorphology, 74(1-4), 17-28.

Lee, M.-J., Kang, J.-e., & Jeon, S. (2012). Application of frequency ratio model and validation for predictive flooded area susceptibility mapping using GIS. Paper presented at the Geoscience and Remote Sensing Symposium (IGARSS), 2012 IEEE International.

Lyu, H.-M., Sun, W.-J., Shen, S.-L., & Arulrajah, A. (2018). Flood risk assessment in metro systems of mega-cities using a GIS-based modeling approach. Science of the Total Environment, 626, 1012-1025.

Miller, J. R. (1990). MORPHOMETRIC ASSESSMENT OF LITHOLOGIC CONTROLS ON DRAINAGE BASIN EVOLUTION IN THE CRAWFORD UPLAND, SOUTH-CENTRAL INDIANA JERRY R. MILLER, DALE F. RITTER,* and R. CRAIG KOCHEL. American Journal of Science, 290, 569-599.

Moore, I. D., Grayson, R., & Ladson, A. (1991). Digital terrain modelling: a review of hydrological, geomorphological, and biological applications. Hydrological processes, 5(1), 3-30.

Mukerji, A., Chatterjee, C., & Raghuwanshi, N. S. (2009). Flood forecasting using ANN, neuro-fuzzy, and neuro-GA models. Journal of Hydrologic Engineering, 14(6), 647-652.

Nampak, H., Pradhan, B., & Manap, M. A. (2014). Application of GIS based data driven evidential belief function model to predict groundwater potential zonation. Journal of Hydrology, 513, 283-300.

Norouzi, G., & Taslimi, M. (2012). The impact of flood damages on production of Iran's Agricultural Sector. Middle East J Sci Res, 12, 921-926.

Oh, H.-J., Kim, Y.-S., Choi, J.-K., Park, E., & Lee, S. (2011). GIS mapping of regional probabilistic groundwater potential in the area of Pohang City, Korea. Journal of Hydrology, 399(3-4), 158-172.

Ozdemir, A. (2011). GIS-based groundwater spring potential mapping in the Sultan Mountains (Konya, Turkey) using frequency ratio, weights of evidence and logistic regression methods and their comparison. Journal of Hydrology, 411(3-4), 290-308.

Pierdicca, N., Pulvirenti, L., Chini, M., Guerriero, L., & Ferrazzoli, P. (2010). A fuzzy-logic-based approach for flood detection from Cosmo-SkyMed data. Paper presented at the Geoscience and Remote Sensing Symposium (IGARSS), 2010 IEEE International.

Polat, K., & Güneş, S. (2006). A hybrid medical decision making system based on principles component analysis, k-NN based weighted pre-processing and adaptive neuro-fuzzy inference system. Digital Signal Processing, 16(6), 913-921.

Pourghasemi, H. R., Mohammady, M., & Pradhan, B. (2012). Landslide susceptibility mapping using index of entropy and conditional probability models in GIS: Safarood Basin, Iran. Catena, 97, 71-84.

Pourtaghi, Z. S., & Pourghasemi, H. R. (2014). GIS-based groundwater spring potential assessment and mapping in the Birjand Township, southern Khorasan Province, Iran. Hydrogeology Journal, 22(3), 643-662.

Pradhan, B. (2010). Flood susceptible mapping and risk area delineation using logistic regression, GIS and remote sensing. Journal of Spatial Hydrology, 9(2).

Pradhan, B. (2013). A comparative study on the predictive ability of the decision tree, support vector machine and neuro-fuzzy models in landslide susceptibility mapping using GIS. Computers & Geosciences, 51, 350-365.

Rahmati, O., Pourghasemi, H. R., & Zeinivand, H. (2016). Flood susceptibility mapping using frequency ratio and weights-of-evidence models in the Golastan Province, Iran. Geocarto International, 31(1), 42-70.

Saidi, S., Ghattassi, A., Anselme, B., & Bouri, S. (2019). GIS Based Multi-criteria Analysis for Flood Risk Assessment: Case of Manouba Essijoumi Basin, NE Tunisia Advances in Remote Sensing and Geo Informatics Applications (pp. 273-279): Springer.

Srivastava, O. S., Denis, D., Srivastava, S. K., Kumar, M., & Kumar, N. (2014). Morphometric analysis of a Semi Urban Watershed, trans Yamuna, draining at Allahabad using Cartosat (DEM) data and GIS. Int. J. Eng. Sci, 3, 71-79.

Tehrany, M. S., Pradhan, B., & Jebur, M. N. (2015). Flood susceptibility analysis and its verification using a novel ensemble support vector machine and frequency ratio method. Stochastic Environmental Research and Risk Assessment, 29(4), 1149-1165.

Tewkesbury, A. P., Comber, A. J., Tate, N. J., Lamb, A., & Fisher, P. F. (2015). A critical synthesis of remotely sensed optical image change detection techniques. Remote Sensing of Environment, 160, 1-14.

Tierney, K. J., Lindell, M. K., & Perry, R. W. (2002). Facing the unexpected: disaster preparedness and response in the United States. Disaster Prevention and Management: An International Journal, 11(3), 222-222.

Tien Bui, D., Khosravi, K., Shahabi, H., Daggupati, P., Adamowski, J. F., M Melesse, A., . . . Bahrami, S. (2019). Flood spatial modeling in northern Iran using remote sensing and gis: A comparison between evidential belief functions and its ensemble with a multivariate logistic regression model. Remote Sensing, 11(13), 1589.

Van Oort, P. (2007). Interpreting the change detection error matrix. Remote Sensing of Environment, 108(1), 1-8.

Volpi, M., Tuia, D., Bovolo, F., Kanevski, M., & Bruzzone, L. (2013). Supervised change detection in VHR images using contextual information and support vector machines. International Journal of Applied Earth Observation and Geoinformation, 20, 77-85.

Walter, V. (2004). Object-based classification of remote sensing data for change detection. ISPRS Journal of photogrammetry and remote sensing, 58(3), 225-238.

Wang, Y.-M., & Elhag, T. M. (2008). An adaptive neuro-fuzzy inference system for bridge risk assessment. Expert Systems with Applications, 34(4), 3099-3106.

Wen, D., Huang, X., Zhang, L., & Benediktsson, J. A. (2016). A novel automatic change detection method for urban high-resolution remotely sensed imagery based on multiindex scene representation. IEEE Transactions on Geoscience and Remote Sensing, 54(1), 609-625.Yang, X.-S. (2009) 'Firefly algorithms for multimodal optimization' International symposium on stochastic algorithms. Springer, pp. 169-178.

Wu, S.-J., Lien, H.-C., & Chang, C.-H. (2010). Modeling risk analysis for forecasting peak discharge during flooding prevention and warning operation. Stochastic Environmental Research and Risk Assessment, 24(8), Yesilnacar, E., & Topal, T. (2005). Landslide susceptibility mapping: a comparison of logistic regression and neural networks methods in a medium scale study, Hendek region (Turkey). Engineering Geology, 79(3-4), 251-266.

Yang, X.-S. (2010). Engineering optimization: an introduction with metaheuristic applications. John Wiley & Sons.

Yilmaz, I. (2010). Comparison of landslide susceptibility mapping methodologies for Koyulhisar, Turkey: conditional probability, logistic regression, artificial neural networks, and support vector machine. Environmental earth sciences, 61(4), 821-836.

Yu, X., & Gen, M. (2010). Introduction to evolutionary algorithms. Springer Science & Business Media.

Yu, J., Qin, X., & Larsen, O. (2013). Joint Monte Carlo and possibilistic simulation for flood damage assessment. Stochastic Environmental Research and Risk Assessment, 27(3), 725-735.1175-1191.

Yuan, F., Sawaya, K. E., Loeffelholz, B. C., & Bauer, M. E. (2005). Land cover classification and change analysis of the Twin Cities (Minnesota) Metropolitan Area by multitemporal Landsat remote sensing. Remote sensing of Environment, 98(2), 317-328.

Zhu, C., & Wang, X. (2009). Landslide susceptibility mapping: A comparison of information and weights-of-evidence methods in Three Gorges Area. Paper presented at the Environmental Science and Information Application Technology, 2009. ESIAT 2009. International Conference on.*Photogrammetry, Remote Sensing and Spatial Information Sciences: 2008 ISPRS Congress Book*. CRC Press, p. 227.

Zhang, J., Gao, B., Chai, H., Ma, Z., & Yang, G. (2016). Identification of DNA-binding proteins using multi-features fusion and binary firefly optimization algorithm. *BMC bioinformatics*, 17(1), 323.

Zhen, L., Wang, L., Wang, X., & Huang, Z. 2 (2008) 'A novel PSO-inspired probability-based binary optimization algorithm' *Information Science and Engineering, 2008. ISISE'08. International Symposium on*. IEEE, pp. 248-251.